ADVANCED FUNCTIONAL MATERIALS
www.afm-journal.de

A Liquid Gripper Based on Phase Transitional Metallic Ferrofluid

Hongzhang Wang, Sen Chen, Haowei Li, Xianzhe Chen, Jiashu Cheng, Yunlin Shao, Chenglin Zhang, Jie Zhang, Linlin Fan, Hao Chang, Rui Guo, Xuelin Wang, Nan Li, Liang Hu, Yen Wei,* and Jing Liu**

Magnetic fields enable dexterous, precise, and real-time control of ferromagnetic materials. However, most materials, including glasses, organics, and metals, are nonmagnetic and often do not respond to a magnetic field. Here, a transitional ferrofluid (TF) made by embedding magnetic iron particles into pure gallium through the treatment of highly concentrated HCl solutions, as well as its switchable interlocking force to objects during the phase change, is introduced to achieve magnetic manipulation of non-magnetic objects. A gripper made by liquid TF enables intimate contact with arbitrarily shaped objects and then generates a strong interlocking force of as high as 1168 N (using only 10 g TF) upon solidification at room temperature, which can be reversibly eliminated (F < 0.01 N) through melting. Owing to electrical conductivity and magnetism, a solid TF can be melted through electromagnetic induction heating. By coupling the switchable physical force during the phase transition and magnetism of TF, embedded non-magnetic objects can be manipulated using an applied magnetic field and become impervious to magnetic stimuli again after heating and releasing the TF. This study is expected to inspire numerous potential applications in the reversible magnetic actuation of soft robotics, remote operation systems, drug delivery, and liquid grippers.

1. Introduction

For centuries, magnetic control has been widely used to accomplish the mechanical manipulation and transport of objects owing to its safe, dexterous, untethered, and real-time controllable properties.[1–3] However, materials with a magnetic susceptibility of close to zero, including glasses, many types of metals, and most organics, often do not respond to a magnetic field.[4] Controlling non-magnetic objects using a magnetic field is important in a broad range of applications in both the scientific and industrial communities.[5] Considerable efforts have been made to achieve this goal by magnetizing non-magnetic materials. As a common strategy, magnetic substances such as Fe, Co, Ni, and NdFeB are combined with non-magnetic targets through physical or chemical treatments.[6–9] For example, the mixing of ferromagnetic particles into an uncured polymer[10,11] and the electroplating of Ni on the surface of the materials[12] are widely employed. Although promising, these magnetizing approaches will change the ingredients and/or damage the original structures of the target objects. In addition, most of these treatments are irreversible, leaving the target materials with magnetism even after manipulation. Consequently, the processed materials with magnetism are prone to interference by the surrounding magnetic

H. Wang, H. Li, J. Cheng, J. Zhang, R. Guo, X. Wang, J. Liu
Department of Biomedical Engineering
School of Medicine
Tsinghua University
Beijing 100084, China
E-mail: jliubme@tsinghua.edu.cn

S. Chen, C. Zhang, L. Fan, H. Chang, N. Li, J. Liu
Beijing Key Lab of Cryobiomedical Engineering and Key Lab of Cryogenics
Technical Institute of Physics and Chemistry
Chinese Academy of Sciences
Beijing 100190, China

S. Chen, C. Zhang, H. Chang, J. Liu
School of Future Technology
University of Chinese Academy of Sciences
Beijing 100049, China

The ORCID identification number(s) for the author(s) of this article can be found under https://doi.org/10.1002/adfm.202100274.

DOI: 10.1002/adfm.202100274

X. Chen
Key Laboratory of Advanced Materials (MOE)
School of Materials Science and Engineering
Tsinghua University
Beijing 100084, China

Y. Shao
Department of Mechanical Engineering
National University of Singapore
Singapore 117575, Singapore

L. Hu
Beijing Advanced Innovation Center for Biomedical Engineering
Institute of Nanotechnology for Single Cell Analysis (INSCA)
School of Biological Science and Medical Engineering
Beihang University
Beijing 100083, China
E-mail: cnhuliang@buaa.edu.cn

Y. Wei
Department of Chemistry
Tsinghua University
Beijing 100084, China
E-mail: weiyen@tsinghua.edu.cn

fields and they are incompatible with instruments such as magnetic resonance imaging machines and scanning electron microscopes. Moreover, the traditional magnetizing approach requires a complicated process and is only suitable for certain groups developing a universal method to control various types of non-magnetic objects using a magnetic field that can overcome the above limitations still remains a formidable challenge for scientific communities.

In this article, we first propose a convenient approach to magnetically manipulate arbitrarily shaped non-magnetic objects by introducing a transitional ferrofluid (TF) by dispersing iron particles into gallium with the help of highly concentrated HCl solutions. It is well known that magnetic materials are either solids that are difficult to deform and reconfigure or ferrofluids with reconfigurable shapes that have difficulty maintaining their structures without external energy.[13] In contrast to traditional magnetic materials, a gallium TF can switch between transformable liquids and extremely rigid solids (with a modulus stiffness of 3.6 GPa) reversibly when stimulated by moderate temperature changes, as schematically shown in **Figure 1**a. Figure 1b and Movie S1, Supporting Information illustrate the magnetic grasp and release of a non-magnetic object with an irregular shape. In a liquid state ($T > T_m = 29.8$ °C), the transformable TF can contact the target objects intimately. After recovering to room temperature ($<T_m$), the TF solidifies and maintains temporary structures with a high stiffness, which can tightly interlock the embedded objects without external energy consumption. Utilizing the magnetism of the TF, the embedded objects can be grasped remotely by a magnetic field ($F_{grasp} > F_{magnetic}$). After delivery to the designated spot, the objects are freed from the bonds by melting the TF again upon moderate heating ($F_{grasp} < F_{magnetic}$). Thus, the magnetic manipulation of arbitrarily shaped objects can be achieved through the phase transition of the TF without other treatments to the target objects. The experimental results show that both the melting and solidifying processes of TF are enhanced compared with pure gallium, which improves the working efficiency of the grasping and release. The mechanism of this phenomenon is also discussed and interpreted. Several experiments were conducted to demonstrate the feasibility

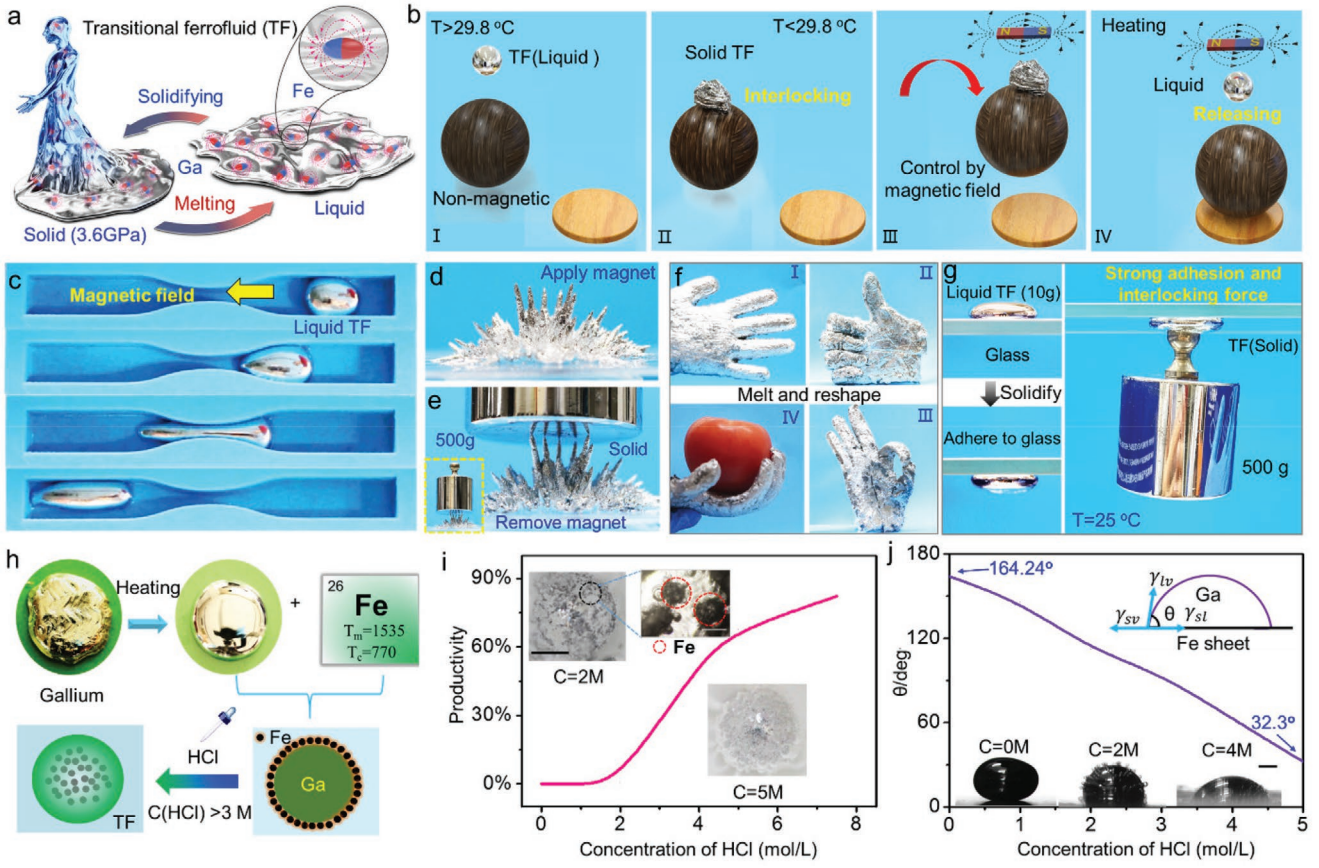

Figure 1. The reversible phase transition of a transitional ferrofluid and its fabrication methods. a) Diagram showing a reversible phase change between a solid and liquid of TF. b) A diagram demonstrating the switchable magnetic grasp of non-magnetic objects by the phase transition of the TF. In a liquid state ($T > T_m = 29.8$ °C), the transformable TF can contact the target objects intimately (I); The TF solidifies at room temperature ($T = 25$ °C $< T_m$) and tightly interlock the embedded objects without external energy consumption (II); Utilizing the magnetism of the TF, the embedded objects can be grasped remotely by a magnetic field (III); After delivery to the designated spot, the objects are freed from the bonds by melting the TF again upon moderate heating (IV). f) The artificial hand made by rubber and TF (I) can mimic the different gestures of a real hand such as "thumbs up(II)", "OK(III)" and grasping the fruit (IV) through melting TF, reshaping and solidifying. g) Solidification of TF enables a strong adhesion force to glass and an interlocking force to the weight (500 g). h) The basic procedure for fabricating a transitional ferrofluid. i) The curves for the productivity of the TF and HCl with different concentrations. j) The curves for the contact angle between gallium and an iron flask with different concentrations of HCl. The scale bar is 2 mm.

of manipulating non-magnetic objects with different shapes using a magnetic field through this liquid gripper. The detailed results of the experiments are discussed below.

2. Transitional Ferrofluids

2.1. Reversibly Switching between Liquid and Solid States

Figure S1, Supporting Information shows the magnetic hysteresis loop of TF and pure gallium at 25 °C, which indicates the significantly enhanced magnetism of TF, whereas there are no net moments of gallium. Considering the transformable characteristics of TF in the liquid state, it is feasible to embed arbitrarily shaped objects with any scale and mechanically interlock them through solidification. Several experiments were conducted to demonstrate that the TF can switch between the excellent transformability of a liquid and the high stiffness of a solid by tuning the temperature. As shown in Figure 1c, the liquid TF droplet can easily transform its shape on a large scale and pass through narrow channels under control of the magnetic field, which might be applied as a magnetically driven transformable robot. An electromagnetic field is applied to generate the desired magnetic field by tuning the voltage. Figure S2a, Supporting Information shows the curves of the magnetic-field strength related to the output voltage. As shown in Figure S2b,c, Supporting Information, the TF moves vertically by changing the voltage of the electromagnet. The moving height of the TF increases continuously with a higher voltage. In particular, TF can jump from the bottom when the electromagnet ($U = 24$ V and $B = 40$ mT) turns on and drop down after turning the power off (Figure S3, Supporting Information). As illustrated in Figure 1d, when a strong magnetic field is applied at the bottom of the liquid TF, the transformable TF presents macroscopic protuberances immediately because of the formation of a chain-like alignment of iron particles.[14] When recovered to room temperature (T = 25 °C) for a certain period of time, the TF solidifies and the newly formed multi-thorn structure is tightly maintained even after the magnetic field has been removed. The Young's modulus of a solid TF at 25 °C can reach ≈3.6 GPa (Figure S4, Supporting Information), and such a multi-thorn structure can bear more than 500 grams of weight (P > 5MPa), as shown in Figure 1e. The multi-thorn structure disappears after heating the TF, and the weight decreases, as shown in Figure S5, Supporting Information. This is different from the previously investigated magnetic field-induced stiffness change in the ferrofluid[15,16], the semi-solid structure of which can achieve a stiffness of approximately several MPa while maintaining its shape under an external magnetic field. By contrast, the solid TF can maintain its original shape in response to a strong magnetic field, whereas the melted TF can transform from a flat interface into a macroscopic protuberance in response to the same magnetic field, which indicates the high stability of a solid TF, as shown in Figure S6, Supporting Information.

An artificial hand was fabricated with a TF coating on the surface of the elastomer hand mode (Figure S7, Supporting Information). Figure S8, Supporting Information shows that the artificial hand presents a high stiffness, and a finger bears a 500 g weight at room temperature. Upon melting the TF, the hand softens and can be reshaped (Figure S9, Supporting Information), which is maintained by solidifying the TF at room temperature. Therefore, the artificial hand can mimic the different gestures of a real hand and grasp a piece of fruit by reshaping and solidification, as shown in Figure 1f. Owing to the magnetism of the TF, the artificial hand can be manipulated through the magnetic field (Figure S10, Supporting Information). Utilizing this magnetic artificial hand, non-magnetic objects can be grasped by a magnetic field. Interestingly, the TF can also adhere to the smooth surface after solidification, extending its application as a liquid gripper. Movie S2, Supporting Information shows that solidifying only 1.6 g TF can result in strong adhesion to a glass beaker, and melting the TF leads to easy detachment. A liquid TF (10 g, $T > T_m$) was placed on a glass surface, and a weight was also embedded into the liquid TF, as shown in Figure 1g. After solidification, the TF enables a strong interlocking force to the weight and the adhesion force to the glass simultaneously. In addition, the structure and interlocking force can be maintained at room temperature without external energy consumption. The above experimental results reflect the strong magnetism, excellent transformability, high stiffness, and strong adhesion force of the TF. Combining these abilities, the TF can transform into different structures through magnetic manipulation, and the temporary structures can be maintained tightly after a quick solidification at room temperature.

2.2. Fabrication of Transitional Ferrofluids

To fabricate the TFs, the liquid metal gallium was adopted as a temperature-controlled phase change solvent (T_m = 29.8 °C), and the iron particles were selected to achieve magnetism. Figure 1h illustrates the fabrication process of the TF. First, gallium is melted by heating, and ferromagnetic particles are then added on the surface of the gallium. In the HCl solution, the iron particles can be dispersed into gallium after stirring. Experimental results reveal that the dispersion of iron particles into gallium only occurs in a highly concentrated HCl solution. Figure S11, Supporting Information shows that the iron particles are still separated from the liquid gallium after treatment with 2 mol L^{-1} HCl, even for a longer reaction time. Figure 1i depicts the productivity of TF in the HCl solution with different concentrations, and only the HCl solution at more than 3 mol L^{-1} can achieve the iron particles dispersed into gallium. The passivated oxide layer on the surface of both gallium and iron particles can be removed through HCl, thus increasing the intermetallic wetting of Ga and Fe.[17,18] The reaction is as follows:

$$Fe_2O_3 + 6HCl \rightarrow 2FeCl_3 + 3H_2O \quad (1)$$

$$Ga_2O_3 + 6HCl \rightarrow 2GaCl_3 + 3H_2O \quad (2)$$

The intermetallic wettability can be obtained by measuring the contact angle θ. The Young's equation is as follows:

$$\theta = \arccos\left(\frac{\gamma_{sv} - \gamma_{sl}}{\gamma_{lv}}\right) \quad (3)$$

where γ_{sv}, γ_{sl}, and γ_{lv} are the interfacial tensions of a solid–vapor, solid–liquid, and liquid–vapor, respectively, and θ is the contact angle. The contact angle can measure the ability of a liquid to wet a solid, as shown in Figure 1j.

According to the liquid metal endocytosis theory[19], endocytosis between two metallic metals easily occurs with contact angles of smaller than 90° (wetting). To investigate the mechanism of the suspension process, the contact angles were measured at different concentrations of HCl. It is difficult to measure the contact angles of iron particles directly; hence, the contact angle between the liquid metal and the Fe flask in the HCl solution was measured using a contact angle instrument (POWEREACH JC2000D3, China). First, an iron flake was placed in the HCl solutions with different concentrations, and a liquid metal micro droplet is then injected into the iron flake. The contact angles were captured and calculated using the same instrument and software. Figure 1j shows that the contact angle is 164.24° in deionized water, which is a non-wetting state. After adding HCl, the contact angle decreased with in an increase in the HCl concentration. With 5 M HCl, the contact angle was only 32.3°, which indicates good intermetallic wetting. The experimental results are consistent with the theory.

2.3. Accelerating Solidification Process of TF

Microstructural evolution of solidifying gallium and TF was observed through metallographic microscopy. **Figure 2**a and Movie S3, Supporting Information show the condensation nucleus spread and the solidification process of gallium, which takes ≈560 s to solidify completely at 20 °C. The visualized microstructure evolution in Figure 2b suggests that the iron nanoparticles dispersed in the TF provide many crystal nuclei and trigger heterogeneous nucleation of TF during solidification (Movie S4, Supporting Information). Figure 2c shows the average solidifying time required for 1 mL of TF and gallium at 20 °C. The experimental results indicate that the solidification of the TF only takes ≈15.9 s, whereas gallium takes 615 s, which is ≈38.7-times longer under the same condition. The DSC results are consistent with the fact that the solidification point of the TF is higher than that of pure gallium (Figure 2d). Supercooling caused by the freezing of Ga impedes the solidification process.[20] When particles are added to liquid metals, they can act as nucleation centers, allowing liquid metal crystals to grow along the surface of the particles. Thus, liquid metals are much easier to solidify, and the degree of supercooling is reduced.[21] In this work, the addition of iron particles allows the liquid metal crystal to grow on the surface of the iron particles, and the iron particles acted as the nucleating agent for a liquid metal to reduce the degree of supercooling. The energy required for homogeneous nucleation (ΔG_c) and heterogeneous nucleation ($\Delta G_c'$) at temperature T are

$$\begin{cases} \Delta G_c = \dfrac{16\pi\gamma_{LC}^3 T_m^2}{3\Delta H_P^2 (T_m - T)^2} \\ \Delta G_c' = \dfrac{16\pi\gamma_{LC}^3 T_m^2}{3\Delta H_P^2 (T_m - T)^2}\left(\dfrac{2-3\cos\theta+\cos^3\theta}{4}\right) = \Delta G_c f(\theta) \end{cases} \quad (4)$$

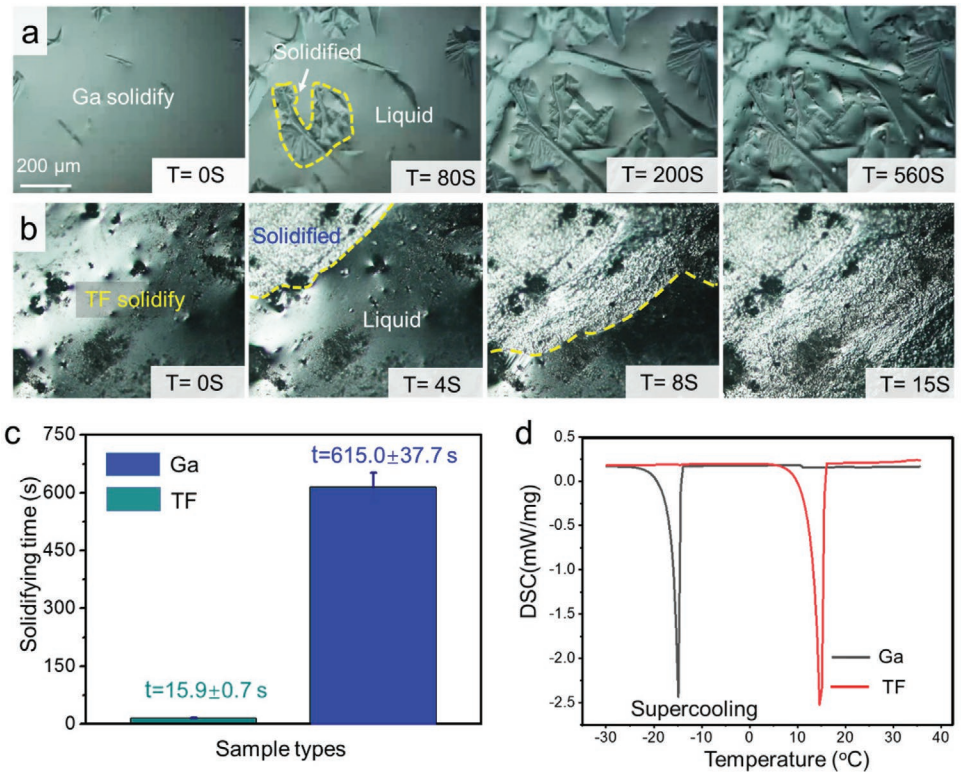

Figure 2. Differences in solidifying process of gallium and TF. Visualized microstructure evolution of a) gallium and b) TF solidification under the metallographic microscope. c) Comparison of solidifying time between gallium and TF. d) DSC curves of gallium and TF during cooling process.

where γ_{LC} is the interface energy of the crystal–liquid gallium, ΔH_P is the volume of the fusion enthalpy, and T_m is the melting point of gallium. Here, the existence of iron particles contributes to the factor $f(\theta)$ in the equation of $\Delta G_c'$. In addition, $f(\theta)$ is a function related to the contact angle θ of gallium and iron particles, the value of which is between zero and 1, as shown in Figure S12, Supporting Information. Thus, the energy required for heterogeneous nucleation at temperature T is lower than that required for homogeneous nucleation, and the TF has a relatively higher nucleating possibility at a higher temperature, which tremendously facilitates the solidification process of the TF. Therefore, the iron particles dispersed inside serve as the nucleating agent and trigger the heterogeneous nucleation of gallium, thereby reducing the supercooling during the solidification process.

2.4. Enhanced Electromagnetic Induction Heating Efficiency of TF

The melting process of a TF induced through heating was also investigated. Gallium has excellent electrical conductivity and can be heated remotely through induced currents in response to an alternating magnetic field (AMF), which is useful in various applications such as tumor hyperthermia[22] and wireless heating of soft robotics.[23] Faraday's law of electromagnetic induction shows that the magnetic flux change in a closed circuit can generate an induced electromotive force (E) in the conductor. The induced E can be described using Faraday's law as follows:

$$\oint_L E \cdot dL = \frac{d}{dt} \iint_S B \cdot dS \tag{5}$$

In addition, the Joule heating can be calculated by

$$Q = i^2 Rt \tag{6}$$

where i is the induced current and R is the resistivity of the TF, and t is the heating time.

From Equations (5) and (6), a magnetic coil can be utilized to generate an eddy current and heat in conductive TF and gallium. A forward-looking infrared system is applied to record the temperature change in gallium. Figure S13, Supporting Information shows that the temperature of the TF increased from room temperature (25 °C) to almost 150 °C (125 °C increase), whereas the pure gallium droplet exhibited an inconspicuous increase (7 °C increase) in temperature with the same heating time (10 s). The heating speed of the TF is ≈18-times faster than that of gallium. The power per unit mass induced by eddy currents is calculated using the following equation[24]:

$$P = \frac{\pi^2 B_P^2 d^2 f^2}{6k\rho D} \tag{7}$$

where B_P is the peak magnetic induction, d is the diameter of the liquid metal droplet, f is the frequency, ρ is the resistivity, and D is the density of the material. In addition, π and k are constants. In our experiments, we assume that d, f, ρ, and D are the same for gallium and TF. Therefore, the difference in the heating effect may be due to the different magnetic inductions of gallium and TF. The magnetic induction B can be calculated using the following equations:

$$B = \mu_r H \tag{8}$$

$$\mu_r = 1 + \chi_m \tag{9}$$

where H is the magnetic field generated by the magnetic coil, μ_r is the relative permeability, and χ_m is the magnetic susceptibility. From the hysteresis loop in Figure S1, Supporting Information, the χ_m of TF is obviously larger than that of pure gallium. According to Equations (7–9), a larger χ_m could lead to a stronger power per unit mass. Therefore, the enhanced heating effect of the TF might result from its higher magnetic susceptibility than that of pure gallium. The simulation model was built to show the heating difference between gallium and TF under an AMF. **Figure 3**a,b shows the simulated heating results of gallium and TF with an AMF for a period of 10 s, which is consistent with our experimental results indicating that the temperature of the TF increases faster than that of pure gallium. Figure 3c shows the melting times of TF and Ga under an AMF. The TF melts immediately, whereas the melting of gallium requires a period of 26 s under an AMF. Therefore, the melting time of the TF is facilitated by 7.6-fold compared with pure gallium.

The temperature change of the TF was too fast to record; hence, we placed the TF into a beaker with water inside and recorded the temperature change of water. In this experiment, the same amounts (10 g) of gallium and TF were placed in a beaker with 40 g of DI water, and the beaker was placed at the center of the magnetic coil. Figure 3d,e shows the temperature change of the beakers with gallium and TF inside, respectively. The initial temperatures of both types of water in the two beakers were the same (24 °C). During electromagnetic induction heating for 60 s, the temperature of water inside the TF increased to 75 °C (51 °C increase), whereas the temperature of water with pure gallium inside increased to 37 °C (13 °C increase). These results demonstrate the significantly facilitated heating efficiency of the TF compared with that of pure gallium. In our supplementary experiment, the same test was also conducted on the Fe particles, which may further illustrate the high heating efficiency of the TF. Figure 3f shows the temperature-heating time curve for water with TF, pure gallium, and iron particles under electromagnetic heating. Unexpectedly, the water temperature with Fe particles barely increased (less than 2 °C) after heating by AMF for 60 s (Figure S14, Supporting Information), which suggests that gallium should also play an important role in such a fast heating. According to Equation (7), the transfer power increases in inverse proportion to the resistivity of the materials. Here, the iron particles are not interconnected to form a conductive pathway, which has a large resistivity and leads to a lower heating efficiency. Therefore, the enhanced heating effect of the TF under the AMF should lie in the high magnetic susceptibility of iron particles and the excellent electrical conductivity of gallium.

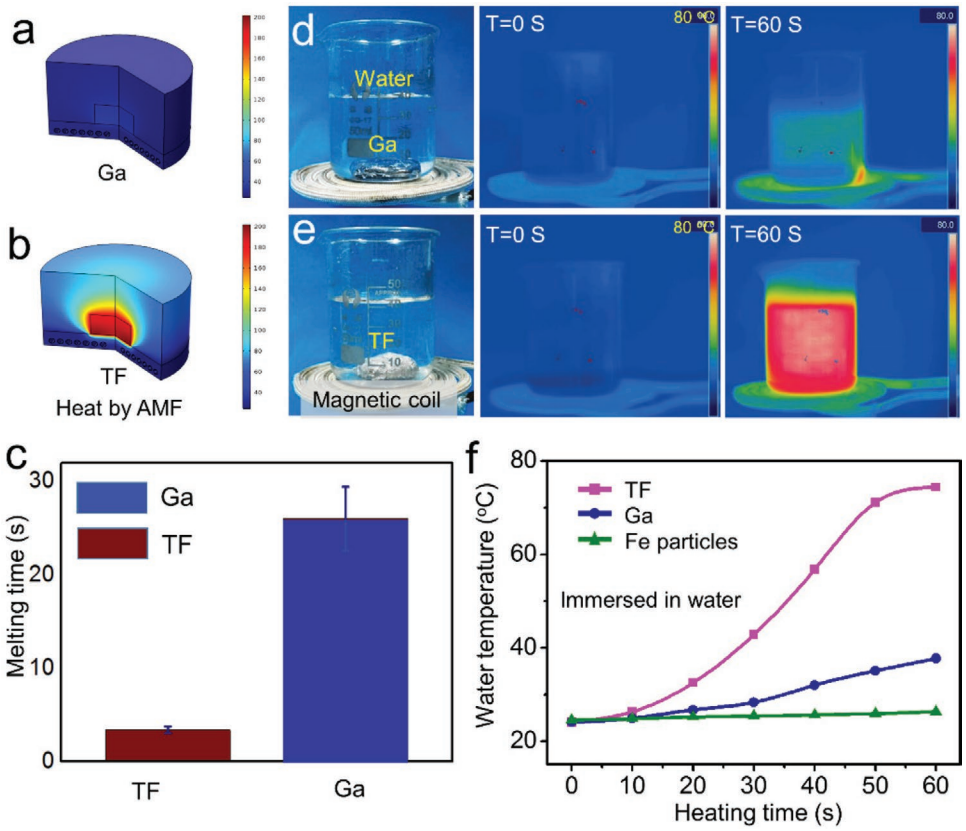

Figure 3. The heating process of gallium and TF under AMF. Simulated heating results of a) gallium and b) TF under AMF for 10 s. c) Comparison of melting time between gallium and TF under the AMF. Here, 10 g of d) gallium and e) TF are immersed in a beaker with 40 g of water, which is placed at the center of the magnetic coil. Infra-red images show the temperatures change of water with the heating by AMF. f) The temperature–time curves for water with different materials inside (TF, Ga, and Fe particles).

2.5. Application as a Liquid Gripper Based on Coupling Phase Transition and Magnetism of TF

As demonstrated in Figure 1b, the phase transition of the TF enables the application of a switchable locking or adhesion force to arbitrarily shaped objects with different scales. Objects with arbitrary shapes can be embedded into a liquid TF and locked by a solidified TF at room temperature. Here, the force used to separate the object (metallic rod) from the solid TF is evaluated using a tension testing machine, which can reach 1168 N when applying 10 g of a solid TF. After melting, the locking force between the rod and liquid TF is reduced to ≈0.01 N. For larger objects with smooth and flat surfaces (such as a glass pane) that cannot be embedded using a TF, the other work mode was applied. The liquid TF is in contact with a part of the surface of the objects and then cooled at room temperature. Gallium oxide (Figure S15, Supporting Information) can be generated between the TF and the surface during the solidification process, enabling a strong adhesion to various surfaces.[25,26] The pull-off force is proportional to $\sqrt{W_{ad}E}$[27], where W_{ad} is the effective work of adhesion, and E is Young's modulus. Therefore, the large Young's modulus of the solid TF (3.6 GPa) enhances the pull-off force. The adhesion force of 10 g TF in a solid state to the contact area can reach 32 N, whereas it decreases to 0.01 N after melting TF, as shown in **Figure 4**a. The TF can adhere to a smooth and flat surface (beaker) against gravity after solidification, as shown in Figure S16, Supporting Information.

Utilizing the magnetism of TF, it is feasible to achieve a magnetic manipulation of non-magnetic objects. The magnetic force F to the iron particles inside is calculated as follows:

$$F = n\nabla(m \cdot B) \tag{10}$$

where n is the number of iron particles (weight ratio), m is the magnetic moment of a particle, and B is the magnetic flux density at the location of the particles. As shown in Figure 4b, the magnetic force F increases with an increase in the magnetic field. In addition, the larger weight ratio of Fe can also generate a larger magnetic force, which is consistent with Equation (10). The grasping force of the TF should be larger than the magnetic attraction force, and the entire system can then be picked by the magnet. After manipulation, the grasp force declines by melting the TF, which is less than the applied magnetic force, causing the separation of objects from the TF. Therefore, the force should satisfy the following equation:

$$F_{grasp}(liquid) < F_{magnetic} < F_{grasp}(solid) \tag{11}$$

According to Figure 4a,b, Equation (11) is satisfied, and therefore the magnetic grasp and release of objects can be achieved.

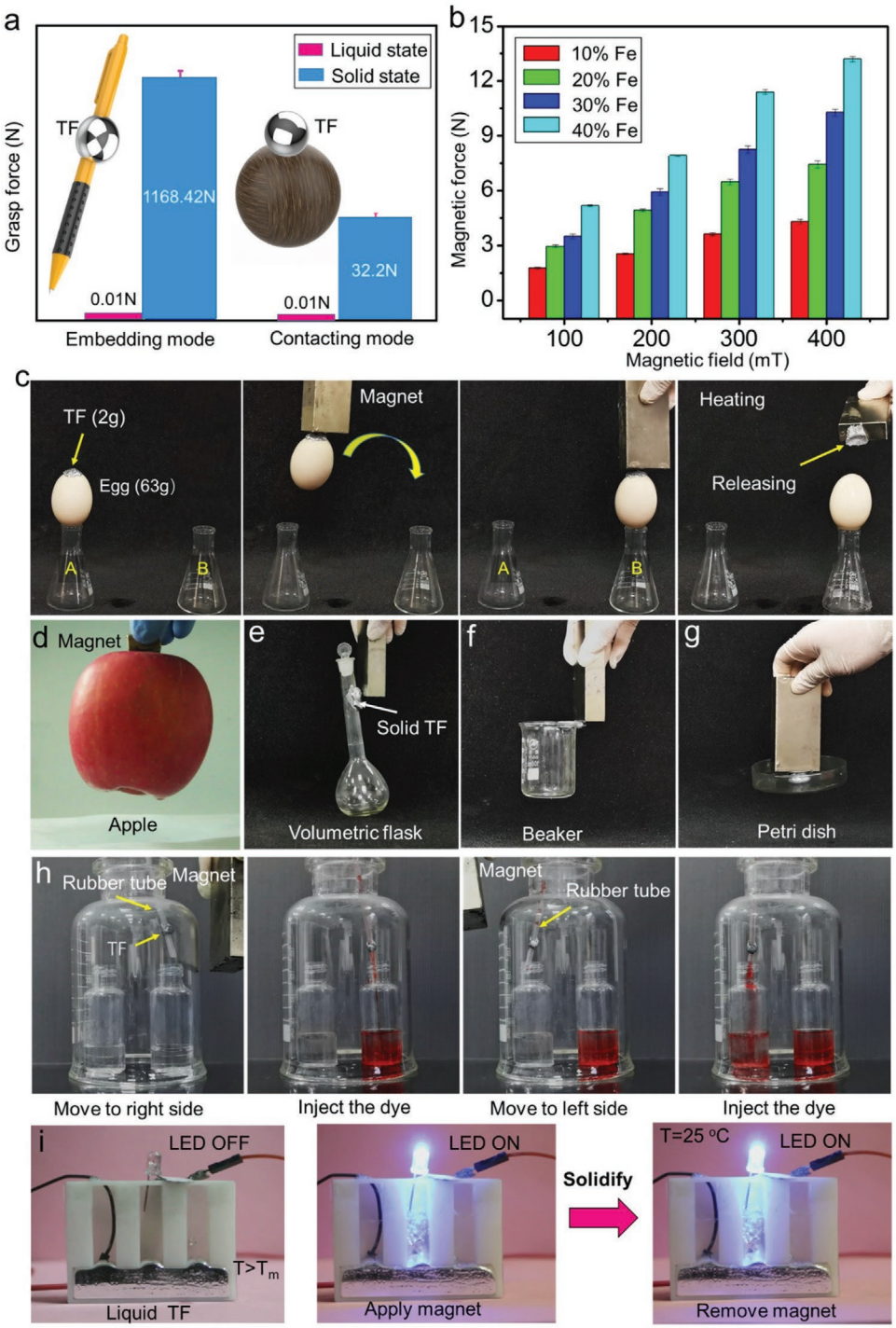

Figure 4. Magnetic control of non-magnetic objects using the phase change in TF. a) Interlocking force (Mode 1) and adhesion force (Mode 2) applied to the objects of TF in liquid and solid states. b) Magnetic attracting force to the TF with different Fe weight ratios under different magnetic fields. c) An egg can be embedded by TF and can then be controlled using a magnet. After manipulation, upon heating, TF melts and releases from the egg. d–g) Magnetic manipulation of non-magnetic objects with different shapes. h) Combining the magnetism of TF, a rubber tube bonded with a solid TF can be manipulated and moved into a target bottle by outside the magnetic field. The red dye can be injected into the bottle through the tube, which can be applied for target drug delivery. i) Intellectual conductors used to connect electrical devices based on the TF. The TF in a liquid state can be stretched and moved by the magnetic field to connect the open circuits, which will maintain the connection after solidification even the magnetic field is removed.

Several experiments have been conducted to demonstrate the magnetic control of different objects with arbitrary shapes. As shown in Figure 4c, 2 g of liquid TF was placed on the surface of an egg (63 g). After cooling at room temperature for a while, TF solidified and adhered to the egg. Therefore, the eggs can be picked and placed at a designated spot using a magnet.

After magnetic manipulation, the TF was heated and melted to release the egg from the magnet. In addition, an apple (250 g) can also be picked up and placed by the magnet using a phase change of 10 g of TF, as shown in Figure 4d. The operating process is also demonstrated in Movie S5, Supporting Information. First, conformal contact between the liquid TF and the apple can be achieved owing to the excellent transformability of TF in the liquid state. After solidification, strong adhesion between the TF and apple is formed, and then the whole apple and TF can be lifted by a magnet. After manipulation, melting the TF would significantly reduce the adhesion force, inducing the detachment of the apple from the TF. The liquid TF is attracted by a magnet and cannot be dropped. Figure 4e–g, and Movie S6, Supporting Information, show that other non-magnetic objects with different shapes can also be controlled by the magnet using the phase change of the TF, which demonstrates significant potential applications in broad fields such as switchable grasping for soft robotics. In addition, Figure S17, Supporting Information demonstrates that the switchable interlocking force still works in water. First, the liquid TF is coated on the ball and then solidifies to generate the interlocking force. The ball floats on the surface of the water in a beaker and immediately drops when a magnet is applied at the bottom. To release the ball from the control of the magnetic field, hot water was added to melt the TF. After warming for 20 s, the ball separated from the melted TF and floated again, and could be applied as a temperature-magnetic joint control switch. Based on the above properties of the TF, it is possible to apply a targeted drug delivery. As shown in Figure 4h, the TF can bond with the rubber tube after solidification. Using the magnetism of the TF, a rubber tube can be manipulated and moved into a target bottle using an external magnetic field. Therefore, the red dye was injected into the target bottle through a tube. For biomedical applications in the body, if some indwelling rubber no longer needs magnetism, the TF can be heated, and the tube is then released from the TF.

Based on the excellent electrical conductivity, the TF provides exciting opportunities for intellectual conductors to connect electrical circuits by controlling the magnetic field. As the concept of this application, the TF in a liquid state can be stretched and moved by the magnetic field to connect the open circuits, which will maintain the connection after solidification even when the magnetic field is removed (Figure S18, Supporting Information). Figure 4i shows the experimental setup. First, the liquid TF (T = 35 °C) was injected into the vertical channel with two electrodes on the top and bottom. A transformable TF can then be stretched by the applied magnet to touch the ceiling of the channel and connect the two electrodes, lighting up the LED. After recovering to room temperature for a while, the TF solidifies and maintains the connection even after removing the magnetic field.

Despite the promising applications of liquid grippers demonstrated above, as the liquid metals easily adhere to many different objects, a liquid residue should be considered. From Movie S2, Supporting Information, we can see that most magnetic liquid metal can be attracted by a magnet, as shown in Figure S19, Supporting Information. The liquid metal residue on different surfaces, such as glass and plastic, which are in contact with liquid TF, are observed using a metallographic microscope. The present experimental results show that, after contact with the TF, there is a small amount liquid metal residue on the surfaces of glass and plastic, which undergoes a phase change process (Figure S19a,b, Supporting Information). However, the liquid metal residue on an object can be entirely removed by alcohol treatment, and there is no gallium or iron on the contact surface from the XPS results (Figure S19c,d, Supporting Information). Furthermore, the liquid gripper can also be encapsulated by a soft and stretchable membrane. A TF can be injected into a latex glove and maintain both its structure and the interlocking force after solidification, which will overcome the influence of liquid metal residue.

3. Conclusion

In summary, for the first time, a liquid gripper developed by embedding iron particles into pure gallium with the help of highly concentrated HCl solutions has been reported to enable magnetically manipulate objects with arbitrary shapes. The solidification of the TF generates a strong interlocking force of as high as 1168 N (using only 10 g of TF) to the embedded object; in addition, melting the TF upon moderate heating causes a separation of the target object and the TF (F < 0.01 N). Experimental results show that the solidifying process of the TF is 38-times faster than that of gallium, and the melting time of TF is 7.6-times faster than that of gallium when remotely heated by the AMF. The mechanism of accelerating both the melting and solidification processes is interpreted, which is attributed to the iron particle dispersion in the gallium. This liquid gripper can "grasp" non-magnetic objects using two work models: embedding or coating (liquid) and interlocking or adhering (solid). By coupling the switchable force (interlocking or adhering) during the phase transition and magnetism of the TF, embedded non-magnetic objects with arbitrary shapes, such as glasses, eggs, fruits, and elastomers, can be controlled by the applied magnetic field and become impervious to magnetic stimuli again after heating and removal of the TF. This approach is quite universal because it does not damage the components or structure of the target objects, and the magnetizing process is entirely reversible, which is expected to provide a new method for magnetic liquid grippers on non-magnetic objects with arbitrary shapes.

4. Experimental Section

Transitional Ferrofluid Fabrication: Pure gallium (Nanjing Jinmei Gallium, Ltd., 99.999%) was used to fabricate the TF owing to its promising melting point (29.8 °C), which offered a phase change at moderate temperatures. Because gallium is solid at room temperature, gallium must be melted in a glass beaker by heating at a temperature of ≈35 °C. Iron particles with a size of ≈38 µm were added to the surface of the liquid gallium. HCl was then poured into a beaker and mixed uniformly. After the solution became clear from the turbid, all iron particles were dispersed into the liquid gallium or partially dissolved in a solution of hydrochloric acid. Because the amount of gallium was sufficient in this reaction, a permanent magnet was used to attract the liquid TF from the remaining pure gallium. The TF solidified at room temperature and was then washed with DI water to remove the residual

HCl. For different experimental purposes, the fabrication details may be changed, which should be noted in the text. The TF with 25% Fe was selected for most of the experiments and tests because of its magnetism and good transformability.

Characterization: Magnetic hysteresis loops of the TF (25% Fe) and pure gallium were tested using a vibrating sample magnetometer at 298 K. Inductively coupled plasma-atomic emission spectrometry was utilized to detect the iron weight ratio in the TF. The surface elemental composition of the TF was determined using XPS (PHI Quantera II). The results were analyzed using the XPSPEAK41 software. Microstructural evolution photographs of Ga and TF were obtained using a metallographic microscope. The wettability between the liquid metal and the Fe flask in the HCl solution was measured using a contact angle instrument (POWEREACH JC2000D3, China).

Heating Methods: Here, different heating methods to melt the gallium and TF, such as AMF, a water bath, heating box, and heating plate were applied, according to the experimental requirements.

Magnetic Control: Magnets with different strengths (B = 50, 100, 200, 300, and 400 mT) and an electromagnet were applied to manipulate the TF. As shown in Figures S2,S3, Supporting Information, the electromagnet was placed above the TF.

AMF Heating

The electromagnetic induction heater is a self-designed alternating current generator connected to a copper plate coil, which is 6-mm thick and has a diameter of 8 cm and is connected to a water-cooling system. The heater was powered by a 50 V, 50 A constant voltage source (Huawei R4850N6). It was assumed that the sample was a cylinder with a height of 0.8 cm and a bottom surface area of 2 cm^2. The simulated heating results were obtained as follows:

$$j\omega\sigma(T)A+\nabla\times(\mu^{-1}\nabla\times A)=0 \tag{12}$$

$$\rho C_P\frac{\partial T}{\partial t}-\nabla\cdot\kappa\nabla T=Q(T,A) \tag{13}$$

where σ is the electrical conductivity, μ is the relative magnetic permeability, ρ is the density of the materials, C_p is the specific heat capacity, k is the thermal conductivity, and Q is the inductive heating. In addition, $\mu 1 = 4\pi \times 10^{-7}$ H m^{-1}, and $\mu 2 = 200 \times 4\pi \times 10^{-7}$ H m^{-1}.

Test of Mechanical Properties: 10 g of TF was applied to the embedding of a metallic rod. The force required to separate the rod from the solid TF was recorded using a tension testing machine. In a liquid state, the force required to separate the rod was below the detection limit of the dynamometer (0.01 N). For work Mode 2 in Figure 4a, a smooth glass was applied to contact the TF (10 g), where the force was tested using a dynamometer.

Productivity Calculation:

$$P=\frac{W_{TF}}{W_{Ga}+W_{Fe}} \tag{14}$$

Here, W_{TF}, W_{Ga}, and W_{Fe} represent the weights (g) of the TF, Ga, and Fe, respectively. A magnet (B = 100 mT) was applied to extract the TF.

Supporting Information

Supporting Information is available from the Wiley Online Library or from the author.

Acknowledgements

The authors thank Xiaoqi Wang, Minghui Duan, Zhu Xiyu, Guoqing Feng, Ruofan Li, and Nan Dong for their help in collecting the part of experimental data. The authors thank Bernadette Miao for reading and revising the manuscript. This work was supported by the National Nature Science Foundation of China under Key Project # 91748206, Shuimu Tsinghua Scholarship, and Beijing Natural Science Foundation (Grant No. 7202104).

Conflict of Interest

The authors declare no conflict of interest.

Data Availability Statement

Data available on request from the authors.

Keywords

liquid gripper, magnetic control, switchable interlocking force, transitional metallic ferrofluid

Received: January 12, 2021
Revised: April 6, 2021
Published online:

[1] W. Hu, G. Z. Lum, M. Mastrangeli, M. Sitti, *Nature* **2018**, *554*, 81.
[2] Y. Kim, H. Yuk, R. Zhao, S. A. Chester, X. Zhao, *Nature* **2018**, *558*, 274.
[3] J. Rahmer, C. Stehning, B. Gleich, *Sci. Rob.* **2017**, *2*, eaal2845.
[4] R. M. Erb, J. J. Martin, R. Soheilian, C. Pan, J. R. Barber, *Adv. Funct. Mater.* **2016**, *26*, 3859.
[5] A. Harraq, J. Lee, B. Bharti, *Sci. Adv.* **2020**, *6*, eaba5337.
[6] X. Zhang, L. Sun, Y. Yu, Y. Zhao, *Adv. Mater.* **2019**, *31*, 1903497.
[7] L. Cao, D. Yu, Z. Xia, H. Wan, C. Liu, T. Yin, Z. He, *Adv. Mater.* **2020**, *32*, 2000827.
[8] J. Jeon, J.-B. Lee, S. K. Chung, D. Kim, *Lab Chip* **2017**, *17*, 128.
[9] J. Zhang, X. Zhu, M. Zeng, L. Fu, *Adv. Sci.* **2020**, *7*, 2000184.
[10] J. Kim, S. E. Chung, S.-E. Choi, H. Lee, J. Kim, S. Kwon, *Nat. Mater.* **2011**, *10*, 747.
[11] Q. Ze, X. Kuang, S. Wu, J. Wong, S. M. Montgomery, R. Zhang, J. M. Kovitz, F. Yang, J. Qi, R. Zhao, *Adv. Mater.* **2020**, *32*, 1906657.
[12] J. Zhang, R. Guo, J. Liu, *J. Mater. Chem. B* **2016**, *4*, 5349.
[13] K. Raj, B. Moskowitz, R. Casciari, *J. Magn. Magn. Mater.* **1995**, *149*, 174.
[14] W. Wang, J. V. I. Timonen, A. Carlson, D. M. Drotlef, C. T. Zhang, S. Kolle, A. Grinthal, T.-S. Wong, B. Hatton, S. H. Kang, S. Kennedy, J. Chi, R. T. Blough, M. Sitti, L. Mahadevan, J. Aizenberg, *Nature* **2018**, *559*, 77.
[15] L. Ren, S. Sun, G. Casillas-Garcia, M. Nancarrow, G. Peleckis, M. Turdy, K. Du, X. Xu, W. Li, L. Jiang, S. Dou, Y. Du, *Adv. Mater.* **2018**, *30*, 1802595.
[16] P. Testa, R. Style, J. Cui, C. Donnelly, E. Borisova, P. Derlet, E. Dufresne, L. Heyderman, *Adv. Mater.* **2019**, *31*, 1900561.
[17] I. A. Castro, A. F. Chrimes, A. Zavabeti, K. J. Berean, B. J. Carey, J. Zhuang, Y. Du, S. X. Dou, K. Suzuki, R. A. Shanks, R. Nixon-Luke, G. Bryant, K. Khoshmanesh, K. Kalantar-zadeh, T. Daeneke, *Nano Lett.* **2017**, *12*, 7831.
[18] H. Wang, B. Yuan, S. Liang, R. Guo, W. Rao, X. Wang, H. Chang, Y. Ding, J. Liu, L. Wang, *Mater. Horiz.* **2018**, *5*, 222.
[19] J. Tang, X. Zhao, J. Li, Y. Zhou, J. Liu, *Adv. Sci.* **2017**, 4.
[20] S. H. Byun, J. Y. Sim, Z. Zhou, J. Lee, J. Jeong, *Sci. Adv.* **2019**, *5*, eaay0418.
[21] C. Zhang, L. Li, X. Yang, J. Shi, J. Liu, *Int. J. Heat Mass Transfer* **2019**, *148*, 119055.
[22] Y. Yu, M. Eijiro, *iScience* **2018**, *3*, 134.
[23] H. Wang, Y. Yao, X. Wang, L. Sheng, X. Yang, Y. Cui, P. Zhang, W. Rao, R. Guo, S. Liang, W. Wu, J. Liu, Z.-Z. He, *ACS Omega* **2019**, *4*, 2311.
[24] F. Fiorillo, *Characterization and Measurement of Magnetic Materials*, 1st ed., Academic Press, San Diego, CA **2004**.
[25] Q. Wang, Y. Yu, J. Yang, J. Liu, *Adv. Mater.* **2015**, *27*, 7109.
[26] Z. Ye, G. Lum, S. Song, S. t. Rich, M. Sitti, *Adv. Mater.* **2016**, *28*, 5088.
[27] R. Shull, J. Crosby, *J. Eng. Mater. Technol.* **1997**, *119*, 211.